Intrinsic polarization switching mechanisms in $BiFeO_3$

Bin Xu,[1,*] Vincent Garcia,[2] Stéphane Fusil,[2] Manuel Bibes,[2] and L. Bellaiche[1]

[1]*Physics Department and Institute for Nanoscience and Engineering, University of Arkansas, Fayetteville, Arkansas 72701, USA*

[2]*Unité Mixte de Physique, CNRS, Thales, Univ. Paris-Sud, Université Paris-Saclay, 91767 Palaiseau, France*

(Received 13 July 2016; published 14 March 2017)

A first-principles-based effective Hamiltonian technique is used to investigate the polarization switching mechanisms in two polymorphic phases of $BiFeO_3$ having no defects. The switching mechanism is homogeneous for any switching field in the rhombohedral phase, while in the supertetragonal phase it changes from the classical nucleation and domain-wall motion to nucleation-limited switching with virtually no propagation, and then to homogeneous switching with increasing electric field. The first two inhomogeneous switching mechanisms of the supertetragonal phase of $BiFeO_3$ are thus intrinsic in nature, and can be well described by the classical and nucleation-limited switching models, respectively. The reason behind their absence in the rhombohedral phase is also indicated. Moreover, the field-induced changes of switching mechanism within the supertetragonal phase are further elucidated from an energetic point of view.

DOI: 10.1103/PhysRevB.95.104104

I. INTRODUCTION

Polarization switching under an applied electric field in ferroelectric (FE) materials has been intensively studied over many decades, and generates continuous interest for both fundamental understanding and emerging technological devices [1–3]. Different types of switching mechanisms have been observed in experiments, which resulted in the development of several models to explain them. For instance, the classic Kolmogorov-Avrami-Ishibashi (KAI) model [4–6] [Eq. (1) of the Supplemental Material (SM) [7]] was proposed to explain the switching occurring in some ferroelectrics through the process of inhomogeneous nucleation of reversed domains and domain-wall motions—schematized in Fig. 1(a). However, another inhomogeneous switching behavior was also found in $Pb(Zr,Ti)O_3$ [8–12] and $BiFeO_3$ (BFO) [13] thin films, which is represented in Fig. 1(b). Such behavior is well described by the nucleation-limited-switching (NLS) model [see Eq. (2) of the SM [7]] that is based on independent switching dynamics in different areas of the film with limited propagation. Moreover, *homogeneous* switching [which is schematized in Fig. 1(c)], i.e., continuous switching without nucleation of domains, was also realized in ferroelectric films being ultrathin (7 nm or less), where extremely large electric field can be achieved [14–17].

To the best of our knowledge, only a few atomistic simulations have been performed to investigate polarization dynamics in ferroelectrics [18–21], likely because such simulations [especially those involving inhomogeneous switchings of Figs. 1(a) and 1(b)] would require the use of supercells that are too large for first-principles calculations. As a result, several questions remain elusive. For instance, do inhomogeneous switchings naturally involve extrinsic effects (e.g., defects, pre-existing domains, interfaces with electrodes, etc.) or rather can they also intrinsically occur in defect-free materials? In case they do occur in compounds with no defects, are the KAI and NLS models still applicable to describe them? One may also wonder if the *same* system can exhibit the three different kinds of switchings shown in Fig. 1, depending on the magnitude of the applied electric field, and what physical quantity governs this hypothetical field-induced change of switching mechanism. It is also of interest to determine if different structural phases of the same compound can exhibit different switching mechanisms, and, if it is the case, why it is so.

In this article, we aim to shed light on these open questions by using a first-principle-based atomistic technique to study defect-free systems made of the most known room-temperature multiferroic compound, that is BFO. Two phases are investigated: the rhombohedral $R3c$ (R) and the supertetragonal $P4mm$ (T) phases [22]. Remarkably, without defects or pre-existing domains, the switching mechanism in the T phase is found to change with increasing the applied electric field, starting from the nucleation and growth of domains, followed by nucleation limited, to end with homogeneous switching, with the first two steps being well described by the KAI and NLS models, respectively. The reason for the existence of these three different mechanisms within the T phase of BFO, depending on the magnitude of the electric field, is also revealed. Moreover and in contrast to the T phase, the R phase of BFO is found to exhibit a single switching mechanism, that is of the homogeneous type. The microscopic origin of such a difference between the R and T phases is also provided.

This article is organized as follows. A description of the computational method is provided in Sec. II. Section III reports the simulated intrinsic switching mechanisms in the R phase and the T phase, and the underlying physics that can interpret the switching behaviors is discussed. Finally, we summarize the study in Sec. IV.

II. METHODS

To study the switching dynamics in BFO, we adopt a first-principle-based effective Hamiltonian (H_{eff}) method, as described in Ref. [23] and references therein [24–26]. The total energy $E_{\text{BFO}}(\{\boldsymbol{u}_i\},\{\eta_H\},\{\eta_I\},\{\boldsymbol{\omega}_i\},\{\boldsymbol{m}_i\})$ of H_{eff} includes four types of degrees of freedom: (1) the local modes $\{\boldsymbol{u}_i\}$ centered on the B sites (i.e., on Fe ions), which are proportional

*Author to whom correspondence should be addressed. Email address: xubin.physics@gmail.com

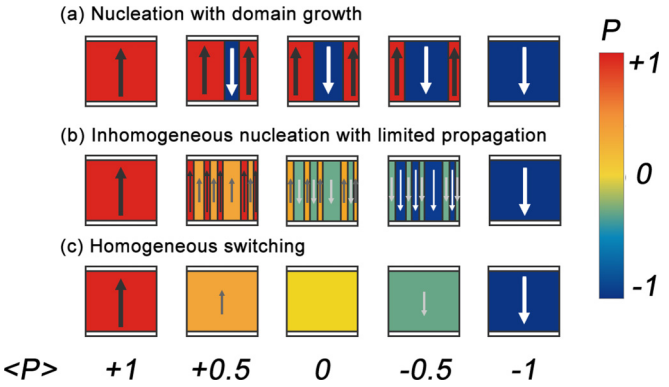

FIG. 1. Schematic illustration of three different switching mechanisms: (a) nucleation followed by domain growth (NDG); (b) nucleation limited (NL); and (c) homogeneous switching (HS). The arrows of different sizes and directions indicate the magnitude and direction of the polarization during switching. Domains of different polarization are illustrated by different colors. The numbers at the bottom denote the average (normalized) polarization.

to the local electric dipole [27,28]; (2) the homogeneous $\{\eta_H\}$ and inhomogeneous $\{\eta_I\}$ strain tensors [27,28]; (3) the pseudovectors $\{\boldsymbol{\omega}_i\}$ that characterize the antiferrodistortive (AFD) oxygen octahedral tiltings [29]; and (4) the magnetic moments $\{\boldsymbol{m}_i\}$ of the Fe ions. (In all cases, the subscript i labels unit cells in our simulated supercells.) Under an applied dc electric field, an additional term $-\sum_i \boldsymbol{p}_i \cdot \boldsymbol{E}_i$ is incorporated, where the local electric dipoles $\boldsymbol{p}_i$ are computed from the product between local modes $\{\boldsymbol{u}_i\}$ and effective charges Z_i^*. This H_{eff} is then used for molecular dynamics (MD) simulations, as detailed in Refs. [30,31], which have successfully reproduced ground-state properties of the bulk $R3c$ phase of BFO in the antiferromagnetic state [30].

The R and T phases are simulated with a $48 \times 48 \times 6$ (containing 69 120 atoms) supercell in terms of the five-atom perovskite cell, to allow mechanisms involving nucleation and/or growth of domains having large *lateral* sizes to occur, if energetically favorable. For the R phase, all strain components are fully relaxed, to model bulk BFO. On the other hand, for the T phase, the in-plane $\eta_{H,1}$ and $\eta_{H,2}$ components (in Voigt notation) of the homogeneous strain are fixed to a -6% strain with respect to their relaxed value in the equilibrium R phase and $\eta_{H,6}$ is imposed to vanish, while other strain components are allowed to relax during the MD simulations—in order to mimic BFO films epitaxially grown on a highly compressive substrate with biaxial stain. MD simulations are carried out at 10 K, in order to minimize thermal fluctuations (note that we numerically found that results at 300 K are qualitatively similar, with slightly shorter switching times).

III. RESULTS AND DISCUSSION

Let us first look at results about the R phase, which is the ground state of BFO under zero or small strain [22]. The initial optimized polarization with no strain is along the [111] direction, and an electric field $\boldsymbol{E}$ of various magnitude, i.e., ranging from 1 to 50 MV cm^{-1}, is applied in the opposite $[\bar{1}\bar{1}\bar{1}]$ direction to the same initial (i.e., $E = 0$) configuration. Figure 2(a) shows the polarization at each $\boldsymbol{E}$ field after equilibration is reached. Technically, a time span of 20 ps is used in the simulations and the average polarization is computed from the last 5 ps of this time span. One can see from Fig. 2(a) that the initial polarization of the R phase is not switched until the electric field is equal to, or larger than, a critical value $E_C = 8$ MV cm^{-1}.

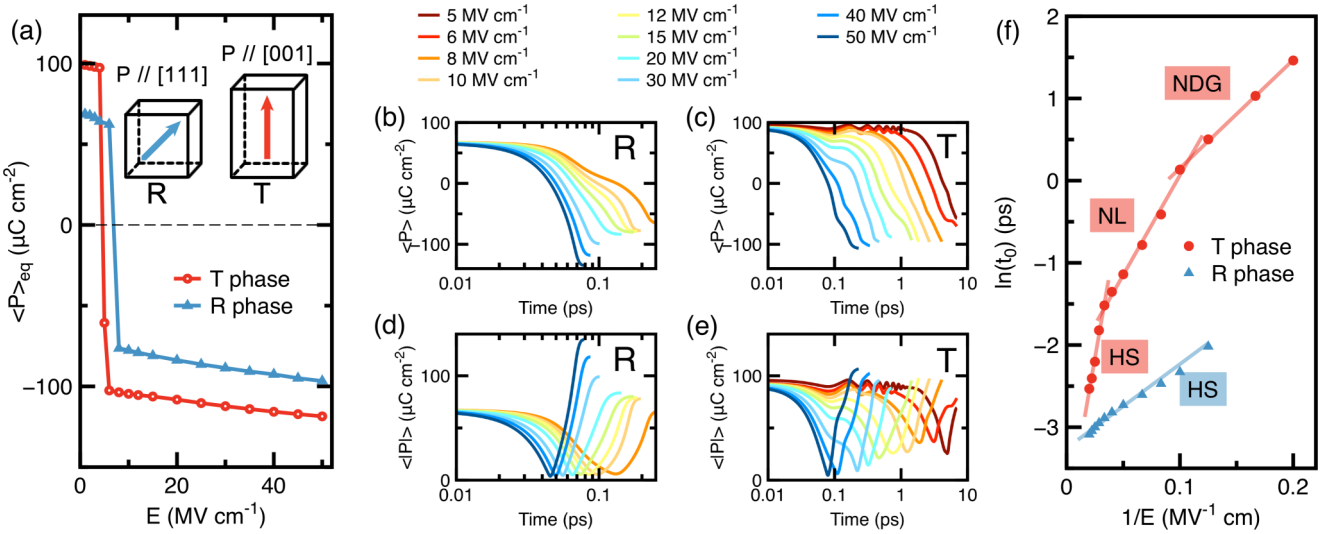

FIG. 2. Properties related to the switching of the polarization. (a) Polarization as a function of electric field after equilibrium is reached. (b)–(e) Time dependence of properties related to electric dipoles during switching under various electric fields. (b,c) Polarization projected along the direction of the applied E field. (d,e) Supercell average of the magnitude of the local electric dipoles. (f) Logarithm of the zero average polarization characteristic time as a function of the inverse of the electric-field magnitude. Discrete points are calculated using MD data, and lines are linear fits to the Merz's law. For the R phase, the initial polarization is along the [111] direction and $\boldsymbol{E}$ is applied along the $[\bar{1}\bar{1}\bar{1}]$ direction. For the T phase, the initial polarization is along the [001] direction and $\boldsymbol{E}$ is applied along the $[00\bar{1}]$ direction.

For electric fields that are capable of switching the initial polarization, the time evolution of the average projected component of the polarization along $\boldsymbol{E}$ (that is, $\langle P\rangle = \frac{1}{V}\sum_i \boldsymbol{d}_i \cdot \boldsymbol{E}/|\boldsymbol{E}|$ with $\boldsymbol{d}_i$ being the local dipole at site i and V being the volume of the whole supercell) is shown in Fig. 2(b). As one can expect, the switching becomes faster with increasing $\boldsymbol{E}$. Moreover, the homogeneity of the switching can be readily deduced from the supercell average of the magnitude of the local dipoles ($\langle|\boldsymbol{P}|\rangle = \frac{1}{V}\sum_i |\boldsymbol{d}_i|$), as shown in Fig. 2(d). In fact, the minimum of each curve reflects how homogeneous the switching is, i.e., the closer $\langle|\boldsymbol{P}|\rangle$ is to zero the more homogeneous the switching is, and interestingly, switching in the R phase is found to be homogeneous across all the field range, as indicated by the minimum of $\langle|P|\rangle$ being close to zero (involving an intermediate state for which all the local dipoles nearly vanish).

The characteristic time t_0 at which $\langle P\rangle$ fully annihilates [Fig. 2(b)] is determined for each field. The resulting linear dependence of $\ln(t_0)$ with $1/E$ in Fig. 2(f) can be fitted to the Merz's law $t_0^{-1} \propto \exp(-E_a/E)$ [32], which confirms that only a single switching mechanism occurs in the R phase [33]. One representative example ($E = 30$ MV cm^{-1}) of the evolution of the polarization switching pattern of the R phase in the (001) plane is shown in Fig. 3(a), and demonstrates again its homogeneous character [34].

The T phase is stable under a -6% epitaxial strain, and it has an initial polarization $+\boldsymbol{P}$ along the [001] direction [35–39]. An electric field is applied along the [00$\bar{1}$] direction, also to the same initial (i.e., $E = 0$) configuration. As shown in Fig. 2(a), the T phase has a slightly lower critical field $E_C = 5$ MV cm^{-1} (leading to a polarization switching) than the R phase.

The time evolution of $\langle P\rangle$ and $\langle|P|\rangle$ in the T phase are depicted in Figs. 2(c) and 2(e). Unlike the R phase case, the minimum of $\langle|P|\rangle$ shows considerable variation with the electric field: it first increases with E, reaching maximum at about 8 MV cm^{-1}, then decreases with further increase of E. Here, the local dipoles are numerically found to have no significant deviation from the axis aligned along both the initial polarization and applied electric field. As a result, a nonzero minimum of $\langle|P|\rangle$ is associated with inhomogeneous switching. Only at high field the minimum of $\langle|P|\rangle$ becomes close to zero, indicating a change to homogeneous switching. From another point of view, the changing of switching mechanism is also reflected from the fitting of t_0 to the Merz's Law [Fig. 2(f)]. One can identify three linear regimes having clearly different slopes, and possessing activation fields of 13.2, 24.2, and 79.3 MV cm^{-1} for the field range of $E <$ 10 MV cm^{-1}, 10 MV cm^{-1} $< E <$ 30 MV cm^{-1}, and $E >$ 30 MV cm^{-1}, respectively.

Remarkably, these three linear regimes are found to correspond to the three distinctively different switching mechanisms that are schematized in Fig. 1. Evolution of the dipole pattern in the (001) plane for three representative cases are illustrated in Figs. 3(b)–3(d) (the corresponding animations are provided in the SM). For low fields [Fig. 3(b)], one can clearly see that the switching occurs via nucleation of domains (some domains switch earlier than other parts of the system) followed by a lateral growth and coalescence of these domains. For intermediate field strength [Fig. 3(c)], the switching continues to occur in a spatially inhomogeneous manner but no obvious domain-wall motion and domain coalescence can be observed, which is consistent with the picture of nucleation limited switching [40]. For high fields [Fig. 3(d)], however, the switching does not involve any nucleation (homogeneous), which can also be deduced from the nearly vanishing $\langle|\boldsymbol{P}|\rangle$ [Fig. 2(e) for E larger than 30 MV cm^{-1}].

Interestingly, to the best of our knowledge, these three switching mechanisms were also found in measurements [15–17,41,42], albeit not in a single experiment. For instance, Ref. [42] observed in $Pb(Zr,Ti)O_3$ capacitors that the switching

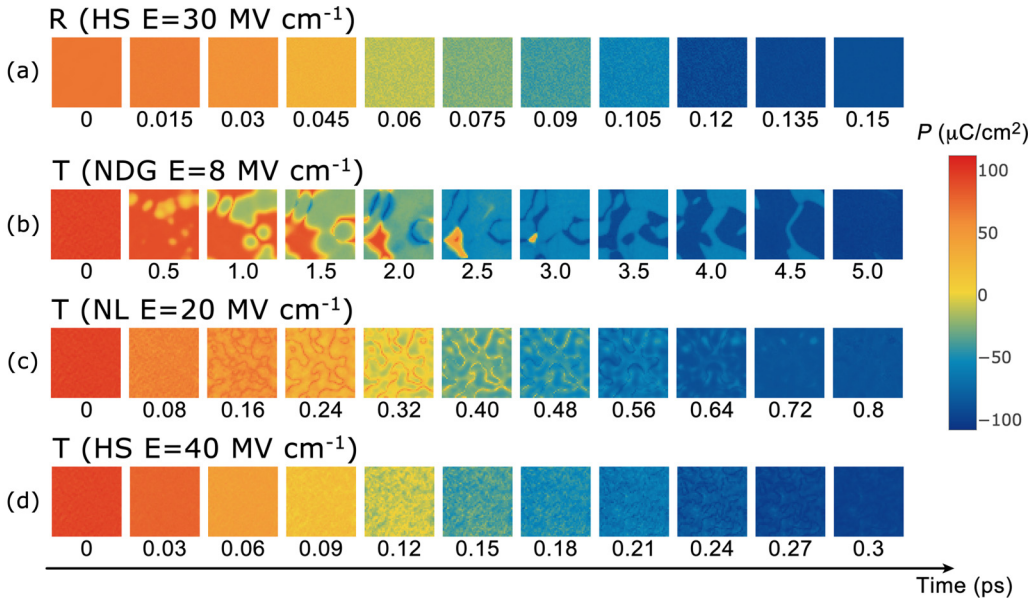

FIG. 3. Predicted evolution of the dipole pattern in the (001) plane for representative cases, simulated with 48 × 48 × 6 supercells: (a) the R phase under $E = 30$ MV cm^{-1}; (b) the T phase under $E = 8$ MV cm^{-1}; (c) the T phase under $E = 20$ MV cm^{-1}; and (d) the T phase under $E = 40$ MV cm^{-1}. The colors (color code) denote different sign and magnitude of the polarization, which is the projected value along the [111] direction for the R phase and along the [001] direction for the T phase. The number below each image is the corresponding time in ps.

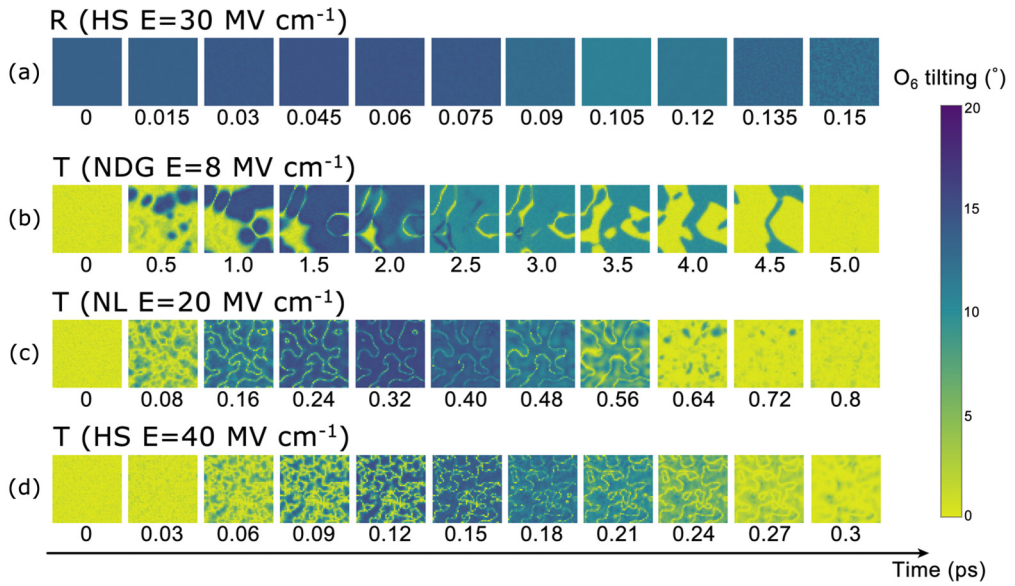

FIG. 4. Predicted evolution of the AFD pattern in the (001) plane for representative cases, simulated with $48 \times 48 \times 6$ supercells: (a) the R phase under $E = 30$ MV cm^{-1}; (b) the T phase under $E = 8$ MV cm^{-1}; (c) the T phase under $E = 20$ MV cm^{-1}; and (d) the T phase under $E = 40$ MV cm^{-1}. The colors (color code) denote different magnitude of the tiltings, which is the projected value (absolute value for better visualization) along the [111] direction for the R phase and along the [001] direction for the T phase. The number below each image is the corresponding time in ps. The corresponding dipolar patterns are shown in Fig. 3.

rate is limited by domain-wall speed at low fields, but nucleation is the rate-limiting mechanism in the high-field range. Moreover, switching without domain formation (i.e., homogeneous switching) was experimentally reported on ultrathin $BaTiO_3$ and $PbTiO_3$ films, in which $\boldsymbol{E}$ reaches the intrinsic coercive field of continuous switching [15–17]. It is worth noting that defects are commonly believed to play a role in inhomogeneous switchings, since nucleation is sensitive to local fluctuations and domain-wall propagation is affected by defects [9–11,41]. Nevertheless, our defect-free simulations imply that the inhomogeneous switching can also be of intrinsic nature.

The fact that the R phase only possesses homogeneous switching for any field above E_C while the T phase was found to exhibit three different switching mechanisms arises from the existence of significant FeO_6 octahedral tiltings in the R phase and their strong coupling with the electric dipoles in BFO. As illustrated in Fig. 4, the FeO_6 octahedral tiltings show closely correlated patterns compared with those of electric dipoles during the switching processes (Fig. 3). As a matter of fact, in the R phase, there exists significant antiphase AFD tiltings about the [111] direction, with these tiltings staying homogeneous and relatively unchanged (and strong) in magnitude during the switching, as shown in Fig. 4(a).[1] On the other hand and as seen in Figs. 4(b)–4(d), the T phase initially possesses vanishing AFD tiltings, due to the strong polarization along the [001] direction and the strong repulsion between this polarization and tiltings about the z axis (due to the positive coefficient involved in a coupling energy between the z component of the oxygen octahedral tiltings and the z component of the polarization [43]). However, intermediate states during the switchings of the T phase adopt regions with small or vanishing polarization (see Fig. 3), which favors the emergence of finite AFD tiltings in these regions (see Fig. 4). The T phase can therefore develop an *inhomogeneous* AFD pattern during the switching, unlike in the R phase. All these facts explain why inhomogeneous dipolar switching occurs in the T phase but not in the R phase.

Moreover, the time dependency of the polarization of the three switching regimes in the T phase is further fitted to the KAI [4–6] and NLS [9] models. As shown in the SM [7], the KAI model provides a better fitting than NLS for the low-field data [corresponding to the nucleation followed by domain growth shown in Fig. S1(b) of the SM [7]], while the NLS model fits better for the intermediate-field case [being associated with nucleation only; see Fig. S1(c) of the SM [7]]. Such findings are consistent with the physical ground of the KAI and NLS models, and demonstrate that such models are also applicable for polarization switching in defect-free materials.

Let us now demonstrate that the switching mechanisms occurring in the R and T phases can be understood from an energetic point of view. For that, let us first realize that, without applying an electric field [i.e., for the $\boldsymbol{E} = 0$ case in the schematized Fig. 5(a)], the $+\boldsymbol{P}$ and $-\boldsymbol{P}$ states are degenerate and separated by an energetic barrier. With increasing the magnitude of $\boldsymbol{E}$ [lower panel of Fig. 5(a)], the $-\boldsymbol{P}$ state, for which the polarization is along the same direction as $\boldsymbol{E}$,

[1]Note that the axis of these tiltings is identical to the direction of the polarization in the R phase because of the strongly negative coefficient involved in a coupling energy between the x and y (respectively, x and z, or y and z) components of the oxygen octahedral tiltings and the x and y (respectively, x and z, or y and z) components of the polarization [43].

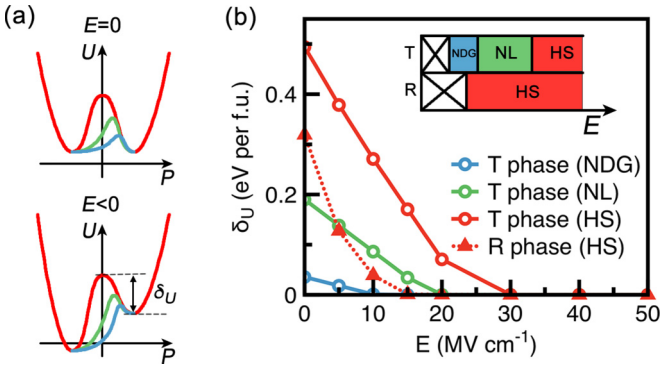

FIG. 5. Energetics related to switching mechanisms. (a) Schematic energy landscape without and with applied $\boldsymbol{E}$ field, for the three identified switching mechanisms: red, green, and blue curves for the HS, NL, and NDG paths, respectively. The initial state is $+\boldsymbol{P}$ for $E < 0$ [for the case of the initial state being $\boldsymbol{P}$ and for $E > 0$, the energy landscape of the right side of panel (a) is reverted with respect to the vertical axis defined by $P = 0$]. (b) Calculated barriers as a function of the electric field. The inset illustrates the switching mechanisms with varying E in the T and R phases.

is favored over the $+\boldsymbol{P}$ state (initial state), since this latter has a polarization that is opposed to the applied field. The barrier height and the energetic variation with respect to P is determined by the path via which the switching occurs. It is intuitive that the homogeneous switching schematized in Fig. 1(c) corresponds to a symmetric energetic path [red curve in the upper panel of Fig. 5(a)]. On the other hand, we numerically find (see the SM [7]) that the paths are asymmetric for the inhomogeneous switching mechanisms schematized in Figs. 1(a) and 1(b). Furthermore, the homogeneous path (to be denoted as HS) has the largest barrier, while the nucleation with domain growth path (to be coined the NDG path) has the lowest barrier. The nucleation-limited path (to be denoted as the NL path) involves a barrier of intermediate magnitude.

With the single HS mechanism, the calculated switching barrier of the R phase is shown in Fig. 5(b). The barrier decreases with increasing E and is estimated to vanish at E slightly above 10 MV cm^{-1}, which agrees well with the critical field of 8 MV cm^{-1} in Fig. 2(a).

For the T phase, the barrier height δ_U decreases for any of the three mechanisms, with respect to the increase of E, because the barrier decreases by the amount of $(\boldsymbol{P} - \boldsymbol{P}_{\text{saddle}}) \cdot \boldsymbol{E}$, where $\boldsymbol{P}$ is the initial polarization and $\boldsymbol{P}_{\text{saddle}}$ is the polarization of the saddle point of the path. For a semiquantitative understanding, we decided to select three different representative paths found in our MD simulations, each associated with a distinct switching mechanism of the polarization of the T phase: the nucleation with domain growth path occurring for $E = 8$ MV cm^{-1}, the nucleation limited path followed at 20 MV cm^{-1}, and the homogeneous path adopted by the T phase when under a field of 40 MV cm^{-1}. As explained in the SM [7], the internal energy of each state involved in these three paths is then computed under various fields ranging from 0 to 50 MV cm^{-1}. The resulting barriers for the NDG, NL and HS paths are found to be equal to 36, 190, and 494 meV/f.u., respectively, at $E = 0$, and then all decrease as E increases until annihilating. This vanishing of these barriers occurs at fields of ~ 10, ~ 20, and ~ 30 MV cm^{-1} for the NDG, NL, and HS paths, respectively. Interestingly, these three latter fields are rather close to the three critical fields of 5, 12, and 30 MV cm^{-1} delimiting the different switching mechanisms found in the MD simulations [see Fig. 2(f) and the inset of Fig. 5(b)]. This similarity is rather remarkable when realizing that some approximations were taken to compute the data of Fig. 5(b) (in particular, we use the same initial, intermediate, and final MD-extracted structures in the NL path for any field), and indicate that the existence of three different and field-dependent switching mechanisms arise from the existence of three different barriers that are annihilated at different electric fields. Moreover, the change of switching mechanism at $E = 12$ MV cm^{-1} (respectively, at $E = 30$ MV cm^{-1}) from NDG to NL (respectively, from NL to HS), despite the fact that the NDG path has (respectively, both NDG and NL paths have) already a zero barrier, can be understood as follows: the adopted switching path is the one that not only involves a low barrier that can be overcome by the thermal energy but also is the shortest in time among all possible paths. For instance and as shown in Fig. 2(f) by extrapolating the fitted straight lines of the NDG and NL mechanisms down to low $1/E$ values, the homogeneous switching of all the dipoles allows, for fields larger than 30 MV cm^{-1}, the fastest annihilation of $\langle P \rangle$ as compared with the inhomogeneous paths.

IV. CONCLUSIONS

In summary, we have discovered that the switching of polarization in the supertetragonal phase of BFO can be *intrinsically* inhomogeneous as well as homogeneous, which mainly depends on the magnitude of the applied electric field. On the other hand, the rhombohedral phase, for which the polarization is strongly coupled to oxygen octahedral tiltings, only exhibits homogeneous switching. These different mechanisms are well explained by the field dependence of the switching barriers as well as the hierarchy of these barriers between different switching processes. It is also worth mentioning that, while the focus of this study is about intrinsic switchings in bulk ferroelectrics, extrinsic effects (such as surface and electrode) can have a *quantitative* effect by modifying the value of critical fields, as suggested by Ref. [44], but not altering the field-induced change of switching mechanisms we presently report, as such change is consistent with the experimental trend of changing mechanisms with respect to the applied field. In some cases, they can also promote inhomogeneous switching over a homogeneous mechanism, as indicated in Ref. [45] because of the presence of interfacial defects.

ACKNOWLEDGMENTS

The authors thank S. Prosandeev for insightful discussions. This work was financially supported by Air Force Office of Scientific Research under Grant No. FA9550-16-1-0065 (B.X.) and the Department of Energy, Office of Basic Energy Sciences, under Contract No. ER-46612 (L.B.). Financial support from the French Agence Nationale de la Recherche (ANR) through the project FERROMON is acknowledged.

[1] J. F. Scott, *Ferroelectric Memories* (Springer-Verlag, Berlin, Heidelberg, New York, 2000), Vol. 3.

[2] M. Dawber, K. M. Rabe, and J. F. Scott, Rev. Mod. Phys. **77**, 1083 (2005).

[3] V. Garcia and M. Bibes, Nat. Commun. **5**, 4289 (2014).

[4] A. N. Kolmogorov, Izv. Akad. Nauk, Ser. Math. **3**, 355 (1937).

[5] M. Avrami, J. Chem. Phys. **8**, 212 (1940).

[6] Y. Ishibashi and Y. Takagi, J. Phys. Soc. Jpn. **31**, 506 (1971).

[7] See Supplemental Material at http://link.aps.org/supplemental/10.1103/PhysRevB.95.104104 for (1) the effect of supercell geometry and size on some results; (2) additional details about our MD results; (3) fitting of our data to the KAI and NLS models; (4) our computed energetic paths; and (5) comparison between theoretical and experimental electric fields.

[8] O. Lohse, M. Grossmann, U. Boettger, D. Bolten, and R. Waser, J. Appl. Phys. **89**, 2332 (2001).

[9] A. K. Tagantsev, I. Stolichnov, N. Setter, J. S. Cross, and M. Tsukada, Phys. Rev. B **66**, 214109 (2002).

[10] A. Gruverman, B. J. Rodriguez, C. Dehoff, J. Waldrep, A. Kingon, R. Nemanich, and J. Cross, Appl. Phys. Lett. **87**, 082902 (2005).

[11] J. Y. Jo, H. S. Han, J.-G. Yoon, T. K. Song, S.-H. Kim, and T. W. Noh, Phys. Rev. Lett. **99**, 267602 (2007).

[12] D. J. Kim, J. Y. Jo, T. H. Kim, S. M. Yang, B. Chen, Y. S. Kim, and T. W. Noh, Appl. Phys. Lett. **91**, 132903 (2007).

[13] S. Boyn, J. Grollier, G. Lecerf, B. Xu, N. Locatelli, S. Fusil, S. Girod, C. Carrétéro, K. Garcia, S. Xavier, J. Tomas, L. Bellaiche, M. Bibes, A. Barthélémy, S. Saïghi, and V. Garcia, Nat. Commun., doi: 10.1038/ncomms14736.

[14] S. Ducharme, V. M. Fridkin, A. V. Bune, S. P. Palto, L. M. Blinov, N. N. Petukhova, and S. G. Yudin, Phys. Rev. Lett. **84**, 175 (2000).

[15] J. Y. Jo, D. J. Kim, Y. S. Kim, S.-B. Choe, T. K. Song, J.-G. Yoon, and T. W. Noh, Phys. Rev. Lett. **97**, 247602 (2006).

[16] M. J. Highland, T. T. Fister, M.-I. Richard, D. D. Fong, P. H. Fuoss, C. Thompson, J. A. Eastman, S. K. Streiffer, and G. B. Stephenson, Phys. Rev. Lett. **105**, 167601 (2010).

[17] R. Gaynutdinov, M. Minnekaev, S. Mitko, A. Tolstikhina, A. Zenkevich, S. Ducharme, and V. Fridkin, Physica B **424**, 8 (2013).

[18] Y.-H. Shin, I. Grinberg, I.-W. Chen, and A. M. Rappe, Nature (London) **449**, 881 (2007).

[19] S. Liu, I. Grinberg, and A. M. Rappe, Appl. Phys. Lett. **103**, 232907 (2013).

[20] R. Xu, S. Liu, I. Grinberg, J. Karthik, A. R. Damodaran, A. M. Rappe, and L. W. Martin, Nat. Mater. **14**, 79 (2015).

[21] S. Liu, I. Grinberg, and A. M. Rappe, Nature (London) **534**, 360 (2016).

[22] D. Sando, B. Xu, L. Bellaiche, and V. Nagarajan, Appl. Phys. Rev. **3**, 011106 (2016).

[23] D. Rahmedov, D. Wang, J. Íñiguez, and L. Bellaiche, Phys. Rev. Lett. **109**, 037207 (2012).

[24] D. Albrecht, S. Lisenkov, W. Ren, D. Rahmedov, I. A. Kornev, and L. Bellaiche, Phys. Rev. B **81**, 140401 (2010).

[25] I. A. Kornev, S. Lisenkov, R. Haumont, B. Dkhil, and L. Bellaiche, Phys. Rev. Lett. **99**, 227602 (2007).

[26] S. Lisenkov, I. A. Kornev, and L. Bellaiche, Phys. Rev. B **79**, 012101 (2009).

[27] W. Zhong, D. Vanderbilt, and K. M. Rabe, Phys. Rev. Lett. **73**, 1861 (1994).

[28] W. Zhong, D. Vanderbilt, and K. M. Rabe, Phys. Rev. B **52**, 6301 (1995).

[29] I. A. Kornev, L. Bellaiche, P. E. Janolin, B. Dkhil, and E. Suard, Phys. Rev. Lett. **97**, 157601 (2006).

[30] D. Wang, J. Weerasinghe, and L. Bellaiche, Phys. Rev. Lett. **109**, 067203 (2012).

[31] S. Bhattacharjee, D. Rahmedov, D. Wang, J. Íñiguez, and L. Bellaiche, Phys. Rev. Lett. **112**, 147601 (2014).

[32] W. J. Merz, Phys. Rev. **95**, 690 (1954).

[33] The slight deviation from the linear fitting is associated with the quantitative degree of inhomogeneity in the "homogeneous" switching for the R phase. The switching gets more homogeneous with larger E field, causing quantitative change of the slope in a rather continuous manner, in contrast to the abrupt change of slope in the case of the T phase.

[34] It is worth noting that we also numerically found (not shown here) that the R-like phase of BFO films being under a -3% epitaxial compressive strain (which is a phase adopting the Cc space group, with a polarization lying along a $[u,u,v]$ direction with $u < v$) also undergoes a homogeneous switching behavior when E is applied along the $[\bar{1}\bar{1}\bar{1}]$ direction.

[35] A. J. Hatt, N. A. Spaldin, and C. Ederer, Phys. Rev. B **81**, 054109 (2010).

[36] B. Dupé, I. C. Infante, G. Geneste, P.-E. Janolin, M. Bibes, A. Barthélémy, S. Lisenkov, L. Bellaiche, S. Ravy, and B. Dkhil, Phys. Rev. B **81**, 144128 (2010).

[37] J. C. Wojdeł and J. Íñiguez, Phys. Rev. Lett. **105**, 037208 (2010).

[38] Z. Chen, S. Prosandeev, Z. L. Luo, W. Ren, Y. Qi, C. W. Huang, L. You, C. Gao, I. A. Kornev, T. Wu, J. Wang, P. Yang, T. Sritharan, L. Bellaiche, and L. Chen, Phys. Rev. B **84**, 094116 (2011).

[39] S. Prosandeev, I. A. Kornev, and L. Bellaiche, Phys. Rev. B **83**, 020102 (2011).

[40] With a thick geometry, i.e., $12 \times 12 \times 72$ supercell, we numerically find that the nucleation occurs not only in the (001) plane but also inhomogeneously along the [001] direction.

[41] Y. W. So, D. J. Kim, T. W. Noh, J.-G. Yoon, and T. K. Song, Appl. Phys. Lett. **86**, 092905 (2005).

[42] S. V. Kalinin and A. Gruverman, *Scanning Probe Microscopy of Functional Materials: Nanoscale Imaging and Spectroscopy* (Springer Science & Business Media, New York, 2010).

[43] I. A. Kornev and L. Bellaiche, Phys. Rev. B **79**, 100105(R) (2009).

[44] G. Gerra, A. K. Tagantsev, and N. Setter, Phys. Rev. Lett. **94**, 107602 (2005).

[45] T. H. Kim, S. H. Baek, S. M. Yang, Y. S. Kim, B. C. Jeon, D. Lee, J.-S. Chung, C. B. Eom, J.-G. Yoon, and T. W. Noh, Appl. Phys. Lett. **99**, 012905 (2011).